Macromolecules

pubs.acs.org/Macromolecules Article

Protonation-Induced Liquid−Liquid Phase Separation and Solid-Like Structural Transformation in Amine-Functional Polyelectrolytes

Shivalika Sharma, Rajat Mukherjee, Mehak Jain, Arindam Chowdhury, and Kamendra P. Sharma*

Cite This: https://doi.org/10.1021/acs.macromol.5c01505 Read Online

ACCESS | Metrics & More | Article Recommendations | Supporting Information

ABSTRACT: Natural polymers having charged groups (polyelectrolytes) form hierarchical structures on complexing with mono- or multivalent counterions. On the contrary, synthetic polyelectrolytes are generally known to undergo complexation with oppositely charged multivalent counter-(macro-)ions. Here, we demonstrate that the simple addition of monobasic acids to an aqueous solution of protonable amine-containing synthetic polyelectrolyte, polyethylenimine (PEI), induces microphase separation, much similar to the macrophase separation observed with the dibasic or tribasic acids. This results in structurally well-defined, metastable, liquid-like droplets of PEI hitherto not observed earlier. The phenomenon is primarily driven by the counterion condensation on charged amine groups and attractive interactions between hydrophobic moieties of the PEI chains. Remarkably, a pH/polarity gradient develops between the surface and the interior of these microdroplets. This leads to slow (∼ few days) sequential protonation (of the PEI chains) that propagates inward from the surface toward the interior of the droplets. The protonation front triggers a curvature change, leading to a morphological transition of the droplets to form anisotropic structures that self-assemble into micron-sized interconnected hollow fibers. Such a phenomenon is generic to other protonable-amine-functional polymers and depends on the valency of the counterion, which dictates the size of phase-separated structures. This study provides the first experimental evidence that even monovalent counterions can mediate complexation with like-charged polyelectrolytes, which drives their liquid−liquid phase separation and subsequent microstructural transformations into fibrils. This model system provides an opportunity for plausible integration of such spatiotemporal dynamics into the synthetic droplets designed to mimic biological systems.

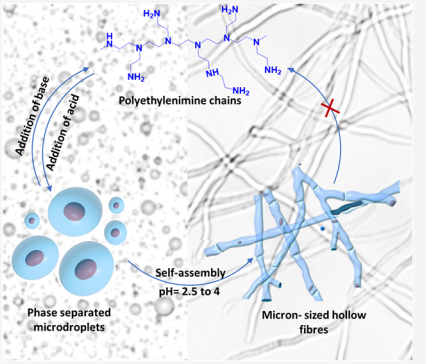

Polymers comprising charged or ionizable groups, also called polyelectrolytes, have been ubiquitous since the origin of life.[1,2] However, unlike their uncharged counterparts, they remain less explored due to the complexities of many factors influencing their solution behavior.[3,4] One of the most intriguing properties of polyelectrolytes is their ability to bind with oppositely charged species, such as ions/macro-ions, leading to the formation of self-assembled polyelectrolyte complexes.[5] The most commonly studied complexes are those formed by mixing oppositely charged polyelectrolytes. On a microscopic or macroscopic level, such self-assembly or complexation can manifest as phase separation—a hallmark of polyelectrolytes.[6] The polymer-rich complexes (with a polymer concentration higher than their surroundings) formed during phase separation can exhibit solid-like or liquid-like properties.[7,8] Notably, the liquid-like synthetic polyelectrolyte complexes, often referred to as "coacervates," have garnered significant attention recently due to their striking similarity to processes that drive surface adhesion by underwater organisms and the biomolecular condensates within cells formed via a liquid−liquid phase separation (LLPS) mechanism.[9−14] LLPS is primarily driven by electrostatic interactions often accompanied by hydrophobic forces, ligand bridging, hydrogen bonding and $\pi-\pi$ interactions.[9,11,12,14] Liquid-like phase-separated systems from synthetic molecules, such as peptides,[8,15−17] polyelectrolytes,[6,18−22] and supramolecular polymers,[23−25] can mimic various properties of biomolecular condensates, viz., high dynamicity, sensitivity toward environmental changes such as pH and temperature, and selective molecular sequestration.[26−28] However, a very important property of maturation or aging of biomolecular condensates from liquid-like to solid-like structures has only been shown for peptide-based coacervates,[29,30] and any such transition has not yet been reported for monofunctional synthetic weak polyelectrolytes.

Intriguingly, complexation is not restricted between oppositely charged macromolecular systems. Natural polyelectrolytes, such as DNA, can form self-assembled structures in the presence of several divalent cations,[31,32] oligo-cations,[32,33] and polycations.[34] Similarly, F-actin, another natural poly-

Received: June 6, 2025
Revised: September 2, 2025
Accepted: November 4, 2025

electrolyte found in the cytoskeleton, organizes into like-charge self-assembly in the presence of Ba^{2+} ions,[35] where the latter act as a zipper system to bind two actin chains by a charge density wave mechanism to form hierarchical filamentous structures. The above-mentioned experimental observations suggest the formation of self-assembled complexes using multivalent counterions that can form ion bridges between like-charged chains and, in combination with short-range hydrophobic interactions, allow attractive interactions between two like-charged polyelectrolyte chains[11]—a phenomenon supported by both simulation and theoretical findings.[36,37] However, few literature reports show the self-assembly of DNA chains by monovalent counterions, e.g., the formation of templated multilayer structures or spherical globules of DNA has been demonstrated by using Na^+, which induces weak attractions between the DNA chains through mechanisms attributed to counterion condensation.[38−40]

In contrast, like-charged synthetic polyelectrolyte complexes driven solely by monovalent counterions and, importantly, also yielding a liquid-like phase separation remain unexplored. This could be due to the lack of requisite correlations between the polyelectrolyte chains by the monovalent counterions. Jain et al.,[41] for the first time, showed that polyethylenimine (PEI), an industrially relevant and an amine-functional, weakly basic, synthetic polyelectrolyte, undergoes unprecedented like-charged self-assembly between pH ∼2.5 to 4 via the addition of various acids, including HCl. The self-assembly mechanism was hypothesized to be a subtle balance of interactions arising from the condensed counterions on partially protonated amines and hydrophobic interactions between the ethylene moieties. Further, under similar pH, covalent modification by less than 0.1% of the primary amines of PEI with fluorophores altered the self-assembly morphology from fibers to sheets.[42] These findings indicated a delicate balance of interactions, where slight chemical perturbations lead to significant changes in self-assembly behavior. However, the exact mechanism and physicochemical picture underlying such self-assembly remain obscure. Through a theoretical study,[43] Muthukumar et al. predicted the formation of microgel-like aggregates due to dipole−dipole interactions between the polymer chains, due to condensed counterions. More recently, using dynamic light scattering,[44] the same group reported a mesomorphic state as precipitates and aggregates in a poly L-lysine bromide and sodium acrylate ion system and, using theoretical calculations, attributed it to dipole−dipole interactions. However, the exact physicochemical understanding of the microscopic structure or the liquid-/solid-like nature of the reported system remained unexplored.

In this study, we bring forward novel insights into the detailed mechanism underlying generic like-charged self-assembly behavior of amine-functional synthetic polyelectrolytes, e.g., polyethylenimine (and polyallylamine), comprising protonable amine groups, triggered by the addition of mono-(HCl), di-(H_2SO_4), or tri-(H_3PO_4) basic acids. We show that depending on the valency of the counterion, the polyethylenimine (PEI) chains undergo a micro- or macrophase separation at a certain window of low pH, driven by a combination of counterion correlations and hydrophobic interactions due to incomplete protonation of the amines. The phase-separated PEI−counterion complexes formed at pH ∼3 show liquid-like droplet behavior reminiscent of coacervates. Further, the droplets exhibit spatial heterogeneity in the protonation, with PEI chains at the surface of droplets showing higher protonation/polarity than those in the interior regions. However, this gradient homogenizes rather slowly and is accompanied by the formation of anisotropic structures that culminate into hollow fibrillar networks. Although multivalent counterion-mediated solid-like aggregate formation has been reported in other polyelectrolyte systems,[35,45−47] such a generic phenomenon of initial liquid-like behavior that dynamically evolves into solid-like and well-defined hierarchical structures upon the addition of acid−based monovalent counterions in a minimalistic system of only synthetic amine-functional polyelectrolyte chains has not been observed experimentally.

RESULTS

Like-Charged Polyethylenimine Phase Separation upon Protonation with Acids. Protonation and counterion-based physiochemical effects on the stability of amine-functional polymers were explored at different pH values with various acids. A synthetic amine-functional polyelectrolyte, branched polyethylenimine (PEI), having M_w = 750 kDa and M_n = 60 kDa, was used for these studies. Branched PEI comprises primary, secondary, and tertiary amines and thus can exhibit a high charge density upon low-pH-based protonation of the amine groups. Therefore, the pH changes in 1−65 μM PEI dilute aqueous and visibly transparent solutions (prepared using Milli-Q water at 25 °C; initially at pH ∼10.6 where the amines are almost unprotonated) were executed by the slow addition of mono-(HCl), di-(H_2SO_4), or tri-(H_3PO_4) basic acids. Different PEI samples with pH values ranging from 9 to 1 were prepared for each acid. Interestingly, while the PEI−HCl samples showed very slight turbidity in the pH range of 4 to 2, the PEI−H_2SO_4 and PEI−H_3PO_4 solutions showed turbidity at distinct pH values. This possibly suggested a microphase separation triggered by HCl, while the dibasic and tribasic acids caused a macrophase separation and formation of large like-charged PEI−counterion complexes (Figure 1).[48,49] The samples were further investigated for the

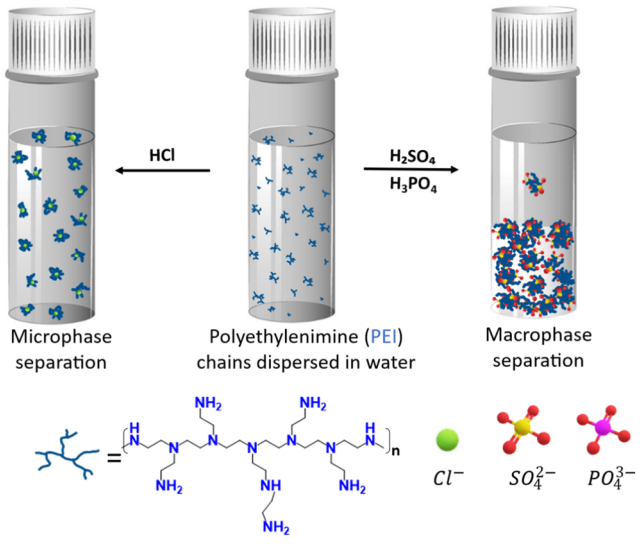

Figure 1. Schematic showing like-charged complex formation by branched polyethylenimine (PEI) chains in a freshly prepared dilute aqueous solution at 25 °C, on the addition of monoprotic or multiprotic inorganic acids. *Note*: The schematic for the PEI chains and the size of the ions is not to scale.

https://doi.org/10.1021/acs.macromol.5c01505
Macromolecules XXXX, XXX, XXX−XXX

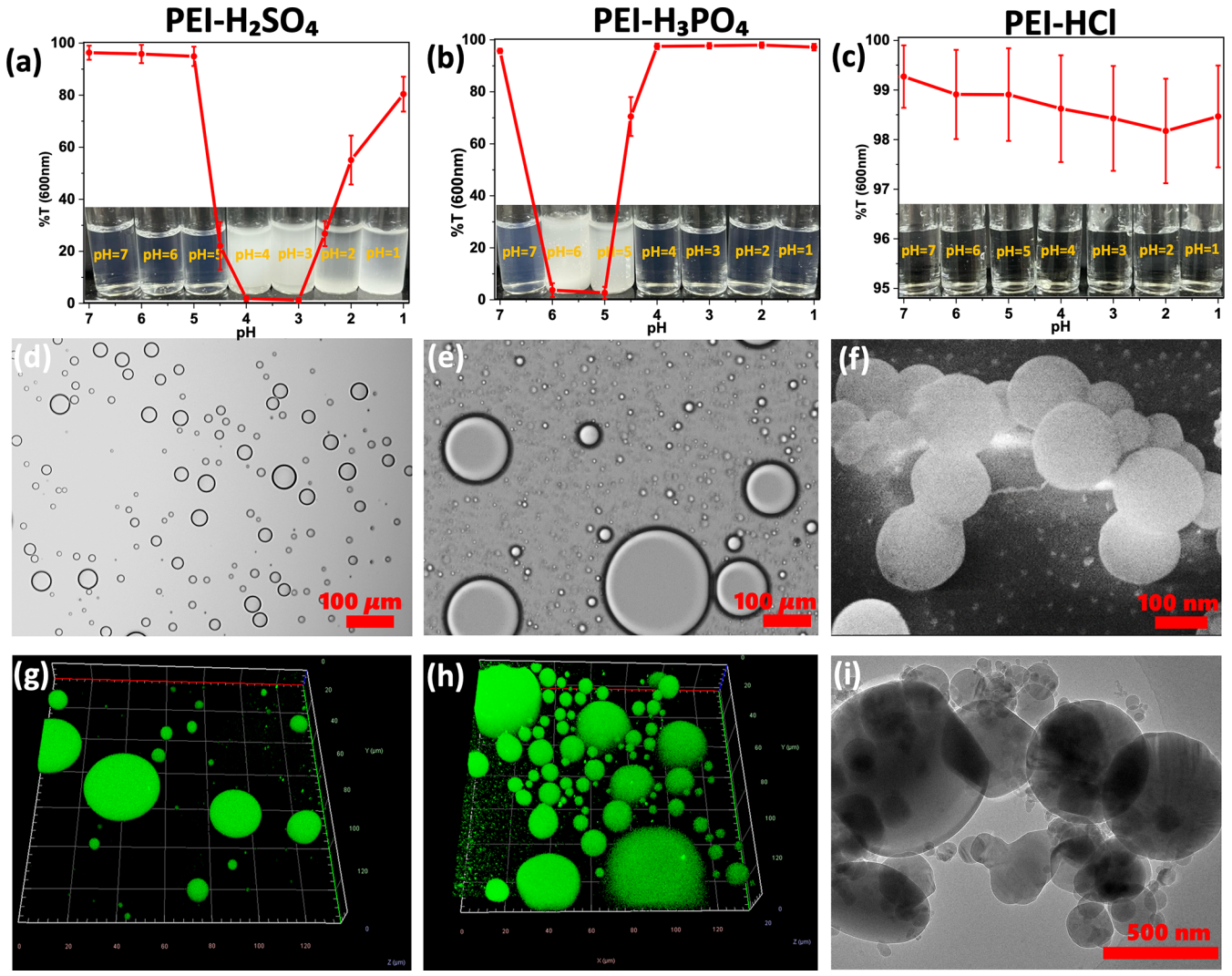

Figure 2. Phase separation investigations of branched polyethylenimine (PEI; 750 kDa) upon protonation using H_2SO_4, H_3PO_4, and HCl. (a–c) Transmittance (%T) studies performed using 600 nm wavelength visible radiation on freshly prepared 65 μM PEI samples with pH ranging from 10 to 1 using 6 N acids: H_2SO_4 (a), H_3PO_4 (b), and HCl (c). The inset shows the corresponding sample solution vials. Turbid solutions of PEI–H_2SO_4 and PEI–H_3PO_4 indicated mobile micrometer-sized structures. (d, e) Bright-field optical micrographs of PEI–H_2SO_4 (pH = 3) and PEI–H_3PO_4 (pH = 5) samples along with their confocal micrographs shown in (g, h), respectively (scale bars for (d), (e) are 100 μm, while for (g), (h) are 136 μm × 136 μm × 20 μm). This indicated that spheroidal structures were the cause of turbidity in these samples. (f) Cryo-SEM micrograph of the PEI–HCl (pH = 3) sample also showed coalescing spheroidal structures. (i) Cryo-TEM micrograph of PEI–HCl (pH = 3) exhibited coalescing spheroids (scale bar for (f) is 100 nm, and (i) is 500 nm).

microscopic structures in the phase-separated samples by performing visible light-based transmittance measurements, optical, confocal, and epi-fluorescence; cryo-electron scanning, and tunneling electron microscopy studies.

Microstructural Understanding of Like-Charged Polyelectrolyte–Counterion Complexes. The phase separation process was monitored through transmittance measurements with a 600 nm wavelength of visible radiation. At pH 10, for all of the samples, the percent transmittance (%T) showed a maximum value of ∼99–100, suggesting transparency. Dropwise addition of a 6 N solution of H_2SO_4 to 65 μM of PEI solution leads to an eye-visible turbidity as the pH decreases below 5 (Figure 2a, inset). This was consistent with the drop in %T from ∼99 at pH 10 to ∼90 at pH 5 (Figure 2a). The transmittance of the samples completely dipped to 0% as the pH was further dropped to 4 and 3. This suggested the formation of larger structures that scattered visible light. However, as the pH dropped below 3, the turbidity began to disappear again, relatively not completely, as can be seen by ∼80%T regained at pH 1. In the case of H_3PO_4, the turbidity from the PEI solution visually appeared at pH below 7, and %T showed a sudden decrease at pH 6 and 5. Visibly, the pH 6 sample showed fast sedimentation of larger structures; however, at pH 5, the turbid sample was relatively more stable. The sample retained turbidity until pH 4.5, below which it became completely transparent, similar to pH 10 samples. In a remarkable observation, when viewed under bright-field optical (Figure 2d,e) and laser scanning confocal microscope (Figure 2g,h), the abovementioned turbidity for PEI–H_2SO_4 and PEI–H_3PO_4 samples was revealed as an outcome of dynamic and coalescing droplets in the solution (Figures S1–S3). The droplets formed by H_3PO_4 were of larger size than those formed from H_2SO_4, e.g., for the most stable turbid solutions, i.e., PEI–H_2SO_4 (pH = 3) and PEI–H_3PO_4 (pH = 5), the optical micrograph-based size distribution analysis of ∼500 droplets provided diameters of 4.4 ± 0.27 μm and 8.9 ±

https://doi.org/10.1021/acs.macromol.5c01505
Macromolecules XXXX, XXX, XXX–XXX

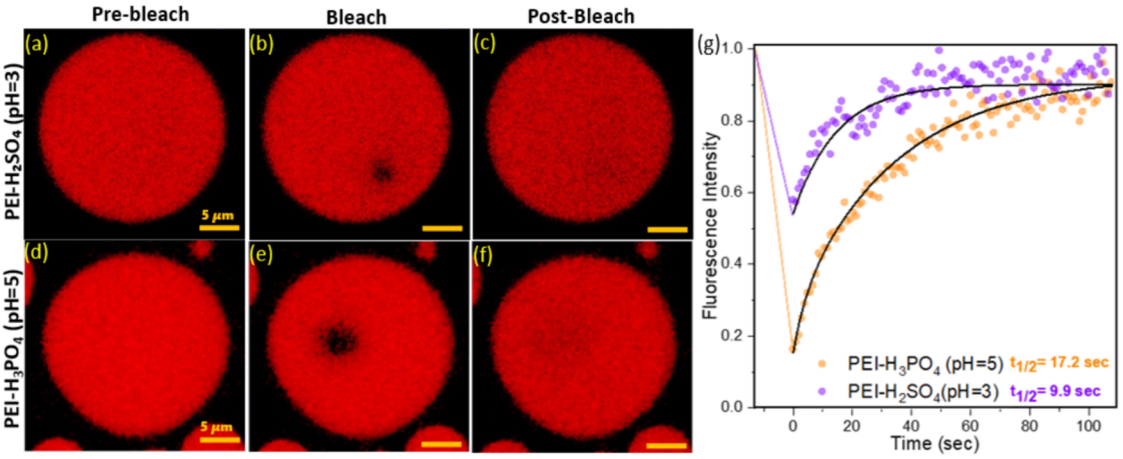

Figure 3. Fluorescence micrographs obtained during FRAP experiments of Alexa Fluor NHS 555-labeled PEI−H_2SO_4 (pH = 3) and PEI−H_3PO_4 (pH = 5) droplet samples. Panels (a, d) represent the droplet images before bleaching, (b, e) represent the droplets at the time of bleaching (the black spots within the droplet indicate the bleached region), and (c, f) represent the images acquired at the end of postbleach recovery, for PEI−H_2SO_4 (pH = 3) and PEI−H_3PO_4 (pH = 5) samples, respectively. Normalization was done to account for background emission and sample bleaching over time. The scale bar for both samples is 10 μm, (g) FRAP curves for (pH = 3) PEI-H_2SO_4 (blue) and (pH = 5) PEI-H_3PO_4 (green) samples are plotted against time.

0.19 μm, respectively (Figure S4). The ζ-potential for PEI−H_2SO_4 (pH = 3) and PEI−H_3PO_4 (pH = 5) droplets was found to be +7.51 mV and +16.3 mV, respectively, indicating like-charged polymer assembly. The detailed size distribution and ζ values are provided in Figure S5. Furthermore, some of the droplets in PEI−H_3PO_4 (pH = 5 and pH = 6) samples also showed multiphasic properties with a polymer-deficient phase encompassed in a polymer-rich phase that was itself embedded in a polymer-deficient phase (Figure S6). The population of multiphasic droplets was predominant in the sedimented phase.

For the PEI−HCl case, the solutions did not show a significant decrease in %T transmittance until pH = 5; however, below this, the overall %T of the solution showed a marginal decline, but the error was significant. The bright-field optical (even at 100×) or fluorescent microscopy measurement could not ascertain the structures; however, the visual appearance of very slight turbidity (in PEI−HCl pH 3 and 4 samples) motivated us to probe the sample with high-resolution microscopy tools. Therefore, cryo-SEM (Figure 2f) and cryo-TEM (Figure 2i) studies were performed on PEI−HCl pH = 3 samples. Intuitively, similar to PEI−H_2SO_4 and PEI−H_3PO_4 samples, these samples also exhibited spheroidal structures/droplets although having relatively much smaller sizes with a cryo-SEM obtained size distribution of ∼25 droplets being 248.1 ± 18.8 nm. This was consistent with the visual and transmittance studies that suggested the formation of smaller-sized polyelectrolyte complexes by PEI and monovalent Cl^- ions, and as reported in our previous studies.[41] The observation of ∼100−200 nm-sized droplets was surprising, as the phenomenon of the formation of like-charged phase-separated complexes/droplets, especially by a weakly basic polyelectrolyte with monovalent counterions, was not known previously.[41] This could be a result of the liquid−liquid phase separation of PEI chains, leading to droplet formation, much similar to what happens in cells for the formation of biomolecular condensates.

To probe the relative intrinsic dynamics of PEI chains within the phase-separated droplets, a fluorescence recovery after the photobleaching (FRAP) experiment was performed by labeling polyethylenimine samples. Alexa Fluor 555 NHS ester dye labeling was done in stock PEI solution at pH = 10.6 before adjusting it to pH = 3 using 6 N H_2SO_4 or pH = 5 using 6 N H_3PO_4. The average fluorescence recovery curve obtained from FRAP measurements (performed in triplicate) on PEI−H_2SO_4 (pH = 3) and PEI−H_3PO_4 (pH = 5) droplets showed that in either case, the droplets did not show 100% recovery in the time frame in which data was recorded. This suggested a spatial restriction, slow molecular dynamics and a viscous environment inside the phase-separated droplets.[48] Further, the mean half-time of recovery obtained on bleaching an area of 2 μm on almost the same-sized droplets of PEI−H_2SO_4 (pH = 3) and PEI−H_3PO_4 (pH = 5) was 9.9 and 17.2 s, respectively, suggesting a liquid-like recovery rate of the droplets (Figure 3). This was consistent with the literature-based observation of similar recovery time from liquid−liquid phase separation (LLPS), e.g., in artificial protocell models and coacervates.[50−52] FRAP experiments further indicated that PEI chains within PEI−H_2SO_4 (pH = 3) droplets exhibited faster dynamics than in PEI−H_3PO_4 (pH = 5) droplets (Figure 3). In both cases, the droplets indicated a dense polymer-rich phase that settled at the bottom of the vial in ∼1 h. Thereafter, the phase-separated and liquid-like bulk/settled PEI−H_2SO_4 (pH = 3) and PEI−H_3PO_4 (pH = 5) samples were analyzed for their flow behavior using shear-sweep rheology (Figure S7). Viscosity measurements as a function of shear rate (0.1−10 s^{-1}) of PEI−H_3PO_4 (pH = 5) exhibited a zero-shear viscosity value of 122.5 Pa·s, with a shear-thinning behavior above 1.6 s^{-1}, whereas the PEI−H_2SO_4 (pH = 3) sample had a zero-shear viscosity value of 4.2 Pa·s and showed shear-thinning behavior above 2.6 s^{-1}. The higher viscosity of PEI−H_3PO_4 (pH = 5) polymer-rich phase could explain their faster sedimentation and was consistent with the FRAP measurements of droplets of the same sample showing slower intrinsic dynamics, compared to that of PEI−H_2SO_4 (pH = 3). Overall, it was astounding to see that these droplets were, in fact, a result of LLPS and could be thought of as a PEI-based simple coacervate system formed by the assembly of like-charged PEI chains assisted by mono/multivalent counterions.

https://doi.org/10.1021/acs.macromol.5c01505
Macromolecules XXXX, XXX, XXX−XXX

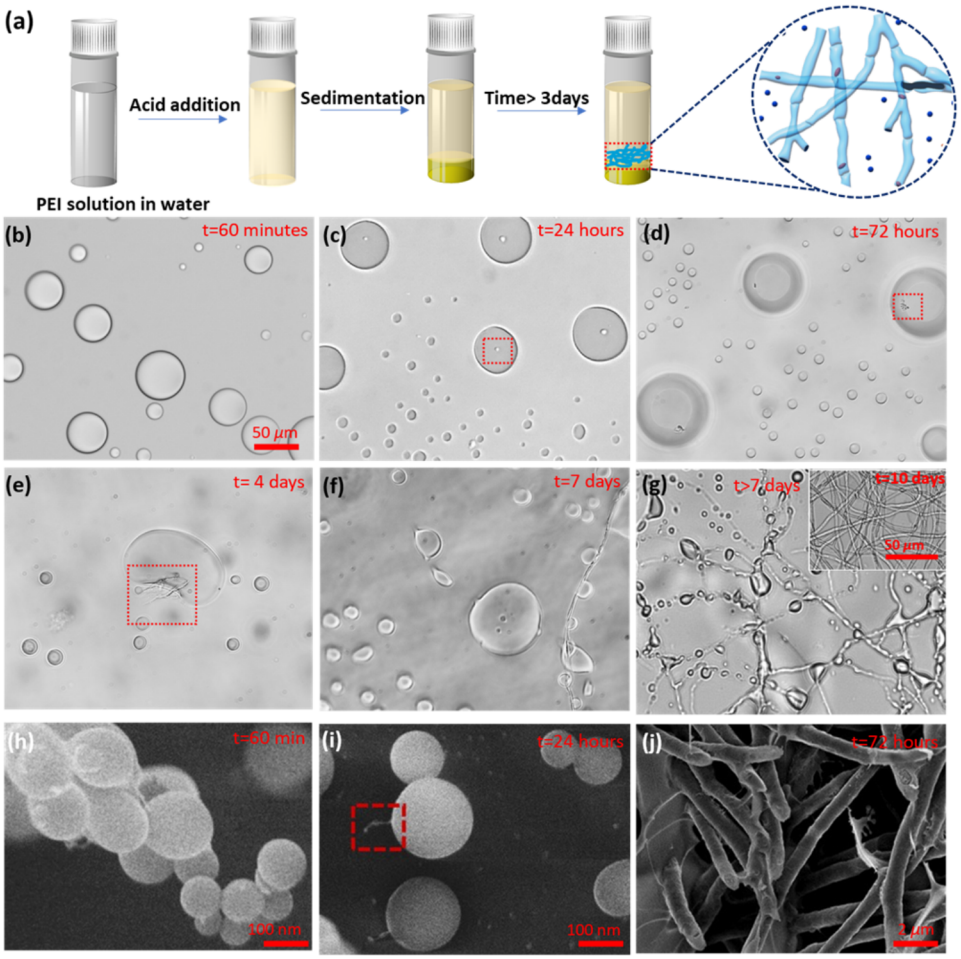

Figure 4. (a) Schematic of the spatiotemporal dynamics occurring in the protonated PEI samples at the interface of polymer-rich and deficient phases. (b–g) Optical micrographs showing time-dependent nucleation and growth of fibrous structures from the phase-separated droplets' surfaces for a 65 μM PEI–H_2SO_4 pH = 3 sample. (h–j) Time-dependent cryo-electron micrographs for PEI–HCl pH = 3 samples. The scale bar for images (b–g) and its inset is 50 μm; for images (h, i), it is 100 nm and (j) is 2 μm.

Charges on the polyelectrolyte chains can be modulated by changing the ionic strength of the solution, which can affect the intrachain and interchain interactions. Therefore, it was imperative to understand the effects of the ionic strength and different kinds of counterions on the phase-separated droplets. Keeping the pH constant, the change in the behavior of PEI–H_2SO_4 (pH = 4 or 3) or PEI–H_3PO_4 (pH = 6 or 5) droplets was studied upon subsequent addition of NaCl. In both cases, the addition of 250 mM NaCl triggered the disappearance of the visually observed turbidity (quantified with a decrease in the transmittance of the bulk solution (Figures S8 and S9)). Consequently, now the droplets were also invisible under the microscope (Figures S8 and S9), indicating that Cl^- ions disrupt the water structure in the polymer-rich phase and probably break the bigger droplets into smaller structures, resulting in a decrease in the turbidity of the solution. This could be understood by the stronger chaotropic effect of Cl^- (as compared to either PO_4^{3-} or SO_4^{2-}), similar to that seen in the case of complex coacervate systems.[53−56] Further, a lower concentration of Cl^- ions was required to trigger the disappearance of PEI–H_2SO_4 (pH = 3) droplets compared to that needed for PEI–H_3PO_4 (pH = 5) droplets. This re-emphasized the lower viscosity (from rheology) and faster dynamics (from FRAP) for the PEI–H_2SO_4 (pH = 3) system as compared to the PEI–H_3PO_4 (pH = 5) system. To ascertain the chain packing in the droplets, S/WAXS studies were employed, and the resultant peaks obtained were fitted by using a correlation-length model (Figure S10). The fitting provided mesh sizes/correlation length (ξ_l); a measure of the distance over which the concentration fluctuation remains correlated), given in Table S1. All of the mesh size values are significantly smaller than the radius of the gyration (R_g; 62 Å) for PEI chains (Figure S11), indicating that the mesh was formed from the overlapping segments of the different PEI chains. Interestingly, the mesh size was minimum for each PEI–acid complex at the pH values which showed higher turbidity or maximum phase separation. These variations in correlation lengths with changes in pH for the PEI–acid complexes highlight the pH-dependent emergence of mesh/domains with variable local densities across the samples.

Spatiotemporal Dynamics of PEI–Counterion Liquid–Liquid Phase-Separated Droplets Result in Structural Transformation to Solid-Like Hollow Fibers. Changing the pH of the PEI solution to 3 using H_2SO_4 leads to phase separation into a polymer-rich and polymer-deficient phase. In an interesting observation, while investigating the phase-separated droplets of PEI–H_2SO_4 solutions having pH 2.5 to 4, the samples showed slow spatiotemporal dynamics in the form of morphological phase transition from droplets to micron-sized hollow fibrillar structures (Figure 4). The fiber

https://doi.org/10.1021/acs.macromol.5c01505
Macromolecules XXXX, XXX, XXX–XXX

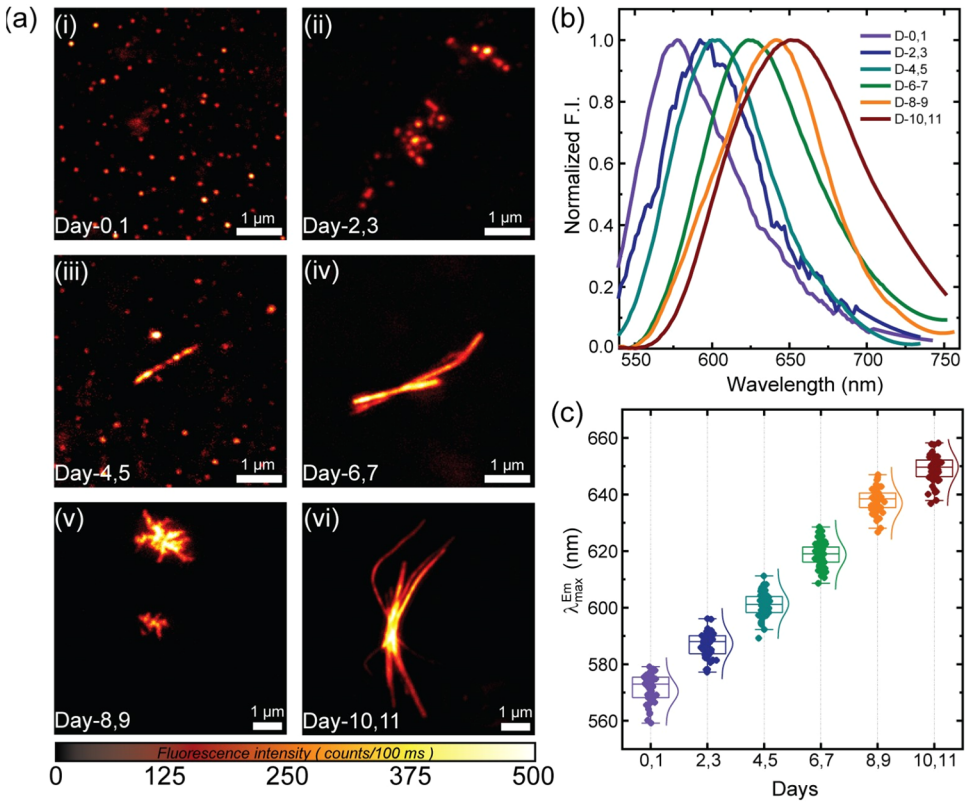

Figure 5. (a) Maximum projection fluorescence intensity images (for 10 s) of PEI stages of growth, observed when stained with NR, (i) Day 0,1: globular forms; (ii) Day 2,3: accumulation of globular forms into microstructures; (iii) Day 4,5: rod-like shapes; (iv) Day 6,7: the appearance of fibrillar forms; (v) Day 8,9: initiation of branching in fibrils; and (vi) Day 10,11: branched fibrils form. (b) Spectra of NR-stained PEI from different days, where Day 0 denotes the preparation of PEI at pH = 3. (c) A bar plot of all the emission spectra of the NR-labeled PEI system collected at different day intervals. (Statistical analysis of 50 regions per time point).

formation was only seen in this pH range, and occurred at the interface of the polymer-rich (sedimented) and the polymer-deficient phase, as shown in the schematic in Figure 4a (original sample vials shown in Figure S12). These could also be observed in situ on a sample sealed in a confocal dish and analyzed for >7 days. Optical micrographs of freshly sealed samples (Figure 4b) showed spheroidal droplet structures for the PEI−H_2SO_4 (pH = 3) sample. The droplets were mobile and could coalesce over time, thereby resulting in bigger droplets. However, after 24 h, small and high-contrast regions (possibly due to changes in the refractive index due to changes in the local concentration of PEI; Figure 4c) emerged in the droplets. After 72 h, these high-contrast regions transformed into protrusions, forming some irregular-shaped structures (Figure 4d).

Similarly, for the PEI−HCl (pH 3) sample, droplets could also be observed using cryo-SEM (Figure 4h); the length scale was different. Interestingly, after 72 h, PEI−HCl (pH = 3) samples showed thin fibers protruding from the surface of the droplets (Figure 4i), thus suggesting that the high-contrast regions seen after 24 h in PEI−H_2SO_4 (pH = 3), Figure 4c, to be the nucleating regions for the fiber formation that protruded from the polymer-rich droplets to polymer-deficient phase. As the irregular structures (seen in Figure 4c) grew into fibers over 4−7 days (Figure 4e,f), the spheroidal droplets from which the fibers protruded, shrank (Figure S12), and their curvature changed to form anisotropic structures. After more than 7 days, many droplets had transformed into thin fibers that connected over the entire sample area, whereby many connecting regions were still seen undergoing morphological transition from droplets to the fibrils (Figure 4g). After 10 days, well-defined and micrometer-sized hollow fibrils could be seen (Figure 4g, inset). In comparison, cryo-SEM of PEI−HCl (pH = 3) after 72 h showed mature fibers with a few microns in diameter and several hundreds of microns in length (Figure 4j). Therefore, it could be thought that as the droplets coalesced and the polymer chains protonated and self-associated, a morphological transition from a spheroidal to fibrillar, coupled with a mechanical transition from a liquid-like to a more solid-like state, also occurred simultaneously. This fibrillation of protonated PEI at pH 3 (2.5−4) was also investigated in the case of H_3PO_4 (Figure S13). It was observed that in the given time frame of observation (a maximum of ∼18−21 days) the fiber formation occurred at pH = 3 and was independent of the type of acid used; however, the diameters varied in the order HCl < H_2SO_4 < H_3PO_4 (Figure S13). This coincided with the well-known buffering properties of PEI seen at low pH values. Interestingly, these fibers were highly robust, solid-like structures, which did not disintegrate even after 24 h upon dilution, addition of salt, or increase in temperature/pH, much in contrast to the liquid-like nature and reversibility of the droplets from which the fibers originated (Figure S14).

While intriguing, the abovementioned morphological transitions could be attributed to the protonation gradient across the cross-section of the droplets. To ascertain this hypothesis, we monitored the spectroscopic signatures of an auxiliary dye molecule incorporated into the droplets over

https://doi.org/10.1021/acs.macromol.5c01505
Macromolecules XXXX, XXX, XXX−XXX

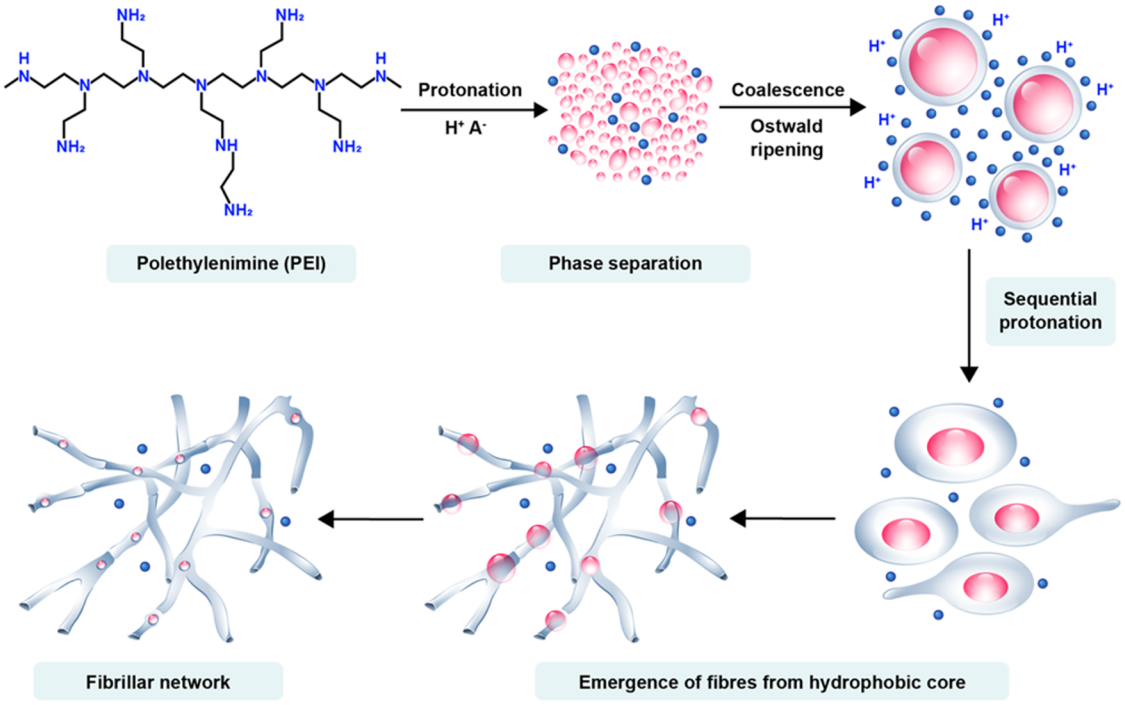

Figure 6. Liquid−liquid phase separation-mediated droplet formation and self-assembly of branched polyethylenimine chains: Schematic illustration depicting the phase separation of the homogeneous PEI solution upon the addition of acids, leading to the formation of smaller droplets with a hydrophobic core can uptake Nile Red dye (shown in red). These smaller droplets undergo fusion and grow in size while simultaneously taking up protons due to a pH gradient between the droplet surface and its interior. Gradually, the inner hydrophobic region is consumed through protonation and chain elongation, leading to the emergence of smaller fibrillar structures that eventually form a larger branched network. As this process progresses, the phase-separated droplets disappear, converting into fibers.

time. Nile Red (NR), a well-known solvatochromic probe,[57] exhibits a progressive red shift in its emission spectrum as the polarity of its surrounding environment increases, making it an effective tool for tracking local polarity changes during different stages of PEI assembly. Being a relatively nonpolar dye, NR was able to effectively stain the PEI droplets as well as larger hierarchical structures (Figure 5a). This enabled us to perform spectrally resolved fluorescence imaging (Figure S15) on individual microstructures stained with NR, thereby obtaining spatially resolved emission spectra of the polarity probe during the various stages of self-assembly (Figure 5b).

Among the tested samples, the PEI−HCl (pH = 3) sample displayed the fastest spheroidal-to-fibrillar transition dynamics and was thus chosen for NR incorporation. After staining a fresh PEI−HCl sample with ∼200 nM NR (Figure S16), fluorescence imaging was performed at various time points ranging from day 0 to 11. In the Day 0−1 sample, the predominant population of diffraction-limited spots (∼200 nm) (Figure 5a(i)) was observed. From Day 2 onwards, distinct structural features began to emerge, as these spots gradually coalesced into larger (400−800 nm) aggregates (Day 2−3, Figure 5a(ii)), which eventually yielded small rod-like structures by Day 4−5 (Figure 5a(iii)). As the process advanced, fibrillar assemblies became prominent (Day 6−7, Figure 5(iv)), which progressively developed into longer, more branched fibrils by Day 8−11 (Figures 5a(v,vi) and S17). Representative spatially resolved fluorescence spectra of NR-stained PEI assemblies, collected during the different stages of growth, are depicted in Figure 5b, clearly revealing a gradual red shift of the entire spectral envelope suggestive of polarity change with time. We quantified the shifts in transition energies by collecting emission spectra from 50 nanodomains at each time point corresponding to the images in Figure 5a and extracted the peak wavelengths (Figure 5c). Our analyses reveal a slight inhomogeneity in the spectral peak positions at each stage of measurement; however, there is a pronounced and consistent red shift in the emission maxima, with mean values from 571.6 (±5.0) nm on Days 0−1 to 648.9 (±4.8) nm by Days 10−11 (Figure 5c). The correlation between the growth of the PEI assemblies and the continuous shift in the transition energies of NR bound to the respective assemblies unambiguously reveals a gradual temporal evolution in the surface polarity. This clearly indicates that the polymer chains transition from a hydrophobic globular state to a relatively more hydrophilic fibrillar form.

DISCUSSION

This study demonstrates that amine-functional polyelectrolytes, such as polyethylenimine (PEI), known for their broad pH buffering capacity, undergo liquid−liquid phase separation upon protonation with mono-, di-, and triprotic acids (Figure 2). The size, morphology, and viscoelastic properties of the phase-separated droplets strongly depend on the counterion valency of the inorganic acid used at a given pH (Figure 2). For instance, H_3PO_4 is a weak acid; its pK_a values are dictated by a weak amine-based polyelectrolyte.[58] At pH > 5, multivalent (PO_4^{3-}, HPO_4^{2-}), and monovalent ($H_2PO_4^-$) ions coexist, which can lead to macrophase separation due to stronger correlations between PEI chains, as shown in the literature for other systems.[59−61] These macrophase-separated droplets show a higher viscosity due to the stronger counterion correlation of trivalent species (compared to divalent ions in PEI−H_2SO_4).[37] However, at pH < 5, H_3PO_4 predominantly

https://doi.org/10.1021/acs.macromol.5c01505
Macromolecules XXXX, XXX, XXX−XXX

exists as a monovalent counterion ($H_2PO_4^-$) in the presence of an amine-functional polymer.[58] The presence of monovalent counterions induces comparatively weaker correlations, resulting in the microphase separation of PEI chains, thus making the bulk solution nearly transparent (Figure 2b). In contrast, H_2SO_4, a strong acid, releases divalent counterions in the solution. However, at pH below 2, PEI−H_2SO_4 samples also show a decrease in turbidity, predominantly due to the re-entrant condensation mechanism[62] of PEI chains due to excess counterions and the resultant ionic repulsions in the solution. In the case of HCl, a strong acid, however, due to monovalent and small Cl^-, a weaker correlation and microphase separation of PEI chains leads to much smaller structures that cannot be observed under an optical microscope due to diffraction limitation. Overall, such phase separation occurs due to interchain correlations between PEI chains, primarily resulting from the counterion condensation onto the protonated-amine groups.

Recent MD simulation studies,[63] on oligomeric PEI chains have shown that as the protonation fraction exceeds 0.43 (equivalent to pH ∼7), Cl^- begin to adsorb onto the PEI chains. A decrease in the potential of mean force (PMF) between two PEI chains at protonation fractions ranging from 0.5 to 0.71 indicates increasing interchain attraction. Notably, the fraction of proximal Cl^- counterions around the PEI chains significantly rises, starting at a protonation fraction of 0.62, reaching its peak at 0.71 (equivalent to pH ∼3 in our case). Since the total number of counterions in the solution remains constant, this apparent increase in proximal counterions suggests counterion sharing between the two chains. However, at higher protonation fractions of 0.8 and 0.9 (equivalent to pH ∼1), the number of proximal counterions decreases again. This has been attributed to a decrease in the chain flexibility.

The phase-separated droplets formed by PEI around pH = 3, irrespective of the acid used, also showed uptake of Nile Red dye, indicating hydrophobic moieties present in the PEI. In fact, PEI is known for its broad pK_a range,[64,65] and the presence of hydrophobic patches.[66,67] These hydrophobic patches are common in proton-sponge-exhibiting amine-functional polymers and contribute to chain interactions and aggregation that can slow the protonation dynamics.

So, what mechanism drives individual PEI chains of $R_g \sim 62$ Å to form fibers with micrometer dimensions by adding acids to decrease the pH within a certain range? Based on the above results and discussion, a pathway/mechanism can be proposed, as shown in Figure 6. Polyethylenimine comprises ethylene units and primary, secondary, and tertiary amine groups within the polymer backbone. The amine groups remain unprotonated at pH = 10. Upon the addition of acids, the PEI chains undergo protonation to develop a nonuniform charge distribution. A counterion condensation follows, causing PEI chains to correlate with contributions from the hydrophobic interaction between ethylene moieties. The result is a phase separation phenomenon that occurs at a certain protonation level,[41] culminating into liquid−liquid phase-separated droplets. Over time, these droplets coalesce and grow, with the droplet surface essentially comprising PEI chains with protonated amine groups (due to pH 3 surroundings) that envelope a hydrophobic core comprising unprotonated PEI chains.[68] Such inhomogeneous protonation behavior (due to conformational effects) for PEI has been previously shown for linear chains, which is likely to be much enhanced for branched PEI. This establishes a pH gradient extending from the outer PEI layers on the droplet surface to the inner core. This is evident from the spatially resolved spectral imaging of NR-stained PEI-H_3PO_4 monophasic droplets, which reveals a polarity gradient from the surface to the core of the droplets (Figure S18). Sequential and slow protonation of amine groups occurring over days induces the extension of PEI chains due to intrachain repulsions, leading to curvature changes within the droplets appearing as fibrillar protrusions from the surface. Simultaneously, the hydrophobic cores keep shrinking in conjunction with the extension and self-association of the PEI chains, leading to hollow structures. However, some hydrophobic cores still remained for up to 14 days of observation. This ultimately transforms the phase-separated droplets into hollow anisotropic rod-like structures (Figure 6). These hollow rods, possibly influenced by depletion interactions,[69] assemble end-to-end, forming a robust three-dimensional network of fibers.

To understand how the nature of amine groups affects the phase separation and spatiotemporal dynamics, other amine-functional polyelectrolytes, e.g., linear polyethylenimine hydrochloride (LPEI·HCl), poly(allyl amine), and poly(diallyl dimethylammonium) hydrochloride (PDDAC·HCl) were also explored (Figure S19). Similar to that in the branched PEI case, for 65 μM aqueous solutions of these polymers, HCl and H_2SO_4 were used to reduce the pH to 3. LPEI−HCl (M_w = 4 kDa; initial pH 2.7), predominantly comprising secondary amines, also formed fibers when NaOH was used to adjust the pH to 3. However, when H_2SO_4 was employed, LPEI−counterion complexes precipitated out of the solution (Figure S20). This suggested that SO_4^{2-} invoked very strong correlations between the LPEI chains, perhaps due to the linear architecture and the lower molecular weight of the polymer. However, these effects could not be deconvoluted further. For another amine-based polyelectrolyte, polyallylamine (PAA; M_w = 17 kDa; initial pH 10.1), also known to show the proton-sponge effect and comprising only primary amine groups, the addition of HCl to reduce the pH to 3 resulted in the formation of fibers after 14 days; however, only solid-like irregular aggregates formed immediately on the addition of H_2SO_4 (Figure S20). This, again, could be attributed to a stronger correlation of primary amines with SO_4^{2-} ions at low pH. In contrast, poly(diallyl dimethylammonium) chloride (PDDAC), comprising completely protonated quaternary amines, did not exhibit phase separation or fiber formation within the observation period of 21 days. The distinct behavior of PDDAC highlights the importance of the requirement of protonable amine-functional groups in driving phase separation upon acidification. This raises an open question and the possibility of exploring other amine-based systems with protonable amine-functional polymers to determine their potential for phase separation and well-structured hierarchical self-assembly under similar conditions.

CONCLUSIONS

We emphasize the subtle role of protonable groups and aliphatic moieties in amine-functional polyelectrolyte chains, which, at low pH, interact via counterion correlations and hydrophobic interactions, respectively. Such interactions give rise to phase-separated droplets comprising polyelectrolyte chains with liquid-like ordering. We further highlight the role of resultant spatial heterogeneity in the local pH within these droplets, which triggers slow dynamics and droplet-to-fiber-like higher-order assemblies. Notably, we show that monovalent

https://doi.org/10.1021/acs.macromol.5c01505
Macromolecules XXXX, XXX, XXX−XXX

counterions from the acid can exhibit significant counterion correlations, previously only reported for multivalent counterparts. This study, therefore, reports a minimalistic system that not only undergoes a liquid−liquid phase separation but subsequently transforms into a solid-like hierarchical structure driven by counterions, even if they are monovalent. This provides novel insights into the fundamental principles governing like-charged polymer self-assembly and, thus, opens new avenues for designing advanced functional materials.

METHODS

Polyelectrolyte Solution Preparation. Polyethylenimine (PEI) solution of the required concentration was prepared by mixing with Milli-Q water and then kept for stirring at room temperature for approximately 6−8 h to ensure maximum dissolution of the polyelectrolyte. The PEI concentration in the stock sample was kept higher to achieve the desired concentration after the acid addition. The acid was added slowly while stirring the solution without letting the temperature exceed 25 °C. The same procedure was followed for polyallylamine and poly(diallyl dimethylammonium chloride). For the linear PEI hydrochloride salt, NaOH was used to maintain the pH, as the original sample had a pH of 2.7.

For labeling with Alexa Fluor NHS 555 and Alexa Fluor NHS 488, a very minute amount of the dye was dissolved in 20 μL of DMSO. The concentration of this solution was determined using a UV−Vis spectrophotometer. This was then added to 70 μM PEI aqueous solution at pH 10.6 by slow dropwise addition in a dark room. The dye-labeled PEI solution was stirred at 8 °C for 24 h. To remove the excess dye, the dye-labeled PEI sample was dialyzed against MiliQ water using a dialysis bag with M_w cut off 10 kDa for 48 h; water was changed every 6 h. The dilution factor of PEI during dialysis was considered by measuring the PEI solution volume in the dialysis bag before and after dialysis.

Characterization. *Optical Microscopy.* For the visualization of samples, an Olympus inverted fluorescence microscope, IX53, was used. The instrument was equipped with a mercury arc lamp as the light source for the fluorescence study, and with an Olympus excitation filter optics (BP 540−550 nm), (BP 418−442 nm), dichroic mirrors (DM 570 nm), (DM 495 nm). Emission barrier filters (BA 575−625 nm) and (LP 542 nm) were used to characterize the Nile Red, Alexa Fluor NHS 555 and FITC-labeled PEI samples, respectively. Approximately 100 μL of PEI sample was drop-cast on a glass slide, covered using a 24 mm coverslip, and then imaged at 4×, 10×, 20×, and 40× magnifications. QImaging MicroPublisher 5.0-RTV color camera (MP5.0-RTV-RCLR10CA) was used to acquire the images, and an Olympus cellSens (CS-ST-V1) imaging software was used for image analysis.

Laser Scanning Confocal Microscopy. 100 μL aliquot of dye-tagged PEI sample was taken in a glass bottom culture dish and observed utilizing a laser scanning confocal microscope (LSM 780, Carl Zeiss, Germany). The observation utilized a range of objectives, including Plan-Apochromat 10×/0.45 NA (air), Plan-Apochromat 40×/1.3 NA (oil), iPlan-Apochromat 63×/1.4 NA (oil), and iPlan-Apochromat 100×/1.4 NA (oil), at ambient temperature. Z-stack images were captured using a photomultiplier tube detector, and for specific cases, the maximum intensity projection was obtained using Zen software.

Cryo-Scanning Electron Microscopy. Imaging of small spheroidal structures and the final fibers was done using the cryo-mode on JEOL JSM-7600F scanning electron microscope. To image freshly prepared samples, PEI solutions of 65 μM concentration were prepared. The pH of the solution was adjusted to 3 by adding 6 N of HCl solution. The resulting solution was immediately centrifuged at 10,000 rpm and 20 °C for 10 min. The residue obtained after centrifugation was drop-cast on carbon-tape-covered copper stubs. Subsequently, the samples were frozen utilizing liquid nitrogen, subjected to platinum sputtering for 15 min, and physically fractured with a knife.

UV−Visible-Based Transmittance Measurements. Transmission measurements were performed by using a Cary 100 UV−visible spectrophotometer to trace the nucleation process in freshly prepared samples. Visible light of 600 nm wavelength was chosen to measure the change in % transmittance of different pH samples over time. Fresh PEI solutions of 65 μM concentration were prepared of pH range 1−10 using HCl, H_2SO_4, and H_3PO_4. All experiments were repeated at least in triplicate.

Fluorescent Recovery after Photobleaching (FRAP). To probe the relative intrinsic dynamics of PEI chains within the phase-separated droplets, fluorescence recovery after photobleaching (FRAP) experiment was performed by labeling polyethylenimine samples. FRAP operates on the deceptively simple principle of irreversibly photobleaching a fluorophore attached to a macromolecule using a high-intensity laser. The intensity of the bleached region is then monitored over time as the bleached molecules exchange with surrounding unbleached molecules in a dynamic system.[52,70] Fluorescent intensity in the selected ROI is plotted versus time to obtain a FRAP curve. Comparing the recovery profile obtained from averaging the data over three different phase-separated droplets for both the samples, half-time of recovery ($\tau_{1/2}$) was calculated. The half-time of recovery ($\tau_{1/2}$) is the time gap between initial bleaching and the point where the sample recovers half of its maximum intensity value.[71]

Alexa Fluor 555 NHS ester dye labeling was done in the stock PEI solution at pH = 10.6 before adjusting it to pH = 3 using 6 N H_2SO_4 or pH = 5 using 6 N H_3PO_4. It should be noted that the concentrations of PEI used in the PEI−H_2SO_4 (pH = 3) sample and PEI−H_3PO_4 (pH = 5) were 65 μM and 30 μM, respectively. In 30 μM PEI−H_2SO_4 (pH = 3) samples, the phase-separated droplet size was much smaller, leading to a significantly low signal-to-noise ratio, while the 65 μM PEI−H_3PO_4 (pH = 5) sample showed jammed droplets. For these experiments, bleached, unbleached, and background intensity data were collected using Zeiss ZEN 3.9 software, and the data were processed using the FrapBOT webtool[72] with double normalization, taking into account the correction for the difference in the initial intensity of the bleached region and loss in overall fluorescence by acquisition bleaching. The data fitted to a single exponential model for PEI−H_2SO_4 (pH = 3) and double exponential model for PEI−H_3PO_4 (pH = 5) samples. The mobile fraction values obtained for PEI−H_2SO_4 (pH = 3) sample and PEI−H_3PO_4 (pH = 5) sample was 0.93 and 0.90, respectively.

ASSOCIATED CONTENT

Supporting Information

The Supporting Information is available free of charge at https://pubs.acs.org/doi/10.1021/acs.macromol.5c01505.

Details of materials used, optical micrographs of PEI using H_2SO_4 and H_3PO_4 acids, coalescence micrographs at different pHs and ionic strengths, size distribution, ζ-potential, rheology-based viscosity measurements of PEI−H_2SO_4 (pH = 3) and PEI−H_3PO_4 (pH = 5) samples, transmittance experiments, S/WAXS measurements, fiber stability experiments under different conditions, microscopy setup schematics for imaging and spectra collection, Nile Red uptake studies, molecular structure for various amine-based polymers and optical micrographs showing their formed fibers and polyelectrolyte complexes on addition of HCl and H_2SO_4. (PDF)

AUTHOR INFORMATION

Corresponding Author

Kamendra P. Sharma − *Department of Chemistry, Indian Institute of Technology Bombay, Mumbai 400076, India;* orcid.org/0000-0002-1932-6698; Email: k.sharma@chem.iitb.ac.in

https://doi.org/10.1021/acs.macromol.5c01505
Macromolecules XXXX, XXX, XXX−XXX

Authors

Shivalika Sharma − *Department of Chemistry, Indian Institute of Technology Bombay, Mumbai 400076, India*

Rajat Mukherjee − *Department of Chemistry, Indian Institute of Technology Bombay, Mumbai 400076, India;* orcid.org/0000-0001-5795-951X

Mehak Jain − *Department of Chemistry, Indian Institute of Technology Bombay, Mumbai 400076, India*

Arindam Chowdhury − *Department of Chemistry, Indian Institute of Technology Bombay, Mumbai 400076, India;* orcid.org/0000-0001-8178-1061

Complete contact information is available at: https://pubs.acs.org/10.1021/acs.macromol.5c01505

Author Contributions

K.P.S. and S.S. conceptualized and designed the research. S.S. carried out the experimental studies, collected/analyzed data, and wrote the initial draft. A.C. and R.M. designed and carried out spectrally resolved fluorescence imaging, and M.J. did the cryo-SEM studies. All the authors discussed the results and contributed towards preparing the final draft of the manuscript.

Notes

The authors declare no competing financial interest.

■ ACKNOWLEDGMENTS

S.S. thanks UGC-JRF for the fellowship and the Department of Chemistry for central facilities. R.M. acknowledges the PMRF and IIT Bombay for fellowship. S.S. also thanks the confocal facility BSBE, SERB-funded Cryogenic TEM National facility at CSIF, IIT Bombay, SAXS facility at RRCAT, Indore, and SAIF, IIT Bombay. S.S. also thanks Rikna TV and Rajat Shukla for their help in PEI−NaCl experiments.

■ REFERENCES

(1) Gilbert, W. Origin of Life: The RNA World. *Nature* **1986**, *319* (6055), 618.

(2) Muthukumar, M. 50th Anniversary Perspective : A Perspective on Polyelectrolyte Solutions. *Macromolecules* **2017**, *50* (24), 9528−9560.

(3) Lopez, C. G.; Matsumoto, A.; Shen, A. Q. Dilute Polyelectrolyte Solutions: Recent Progress and Open Questions. *Soft Matter* **2024**, *20* (12), 2635−2687.

(4) Traeger, A.; Leiske, M. N. The Whole Is Greater than the Sum of Its Parts − Challenges and Perspectives in Polyelectrolytes. *Biomacromolecules* **2025**, *26* (1), 5−32.

(5) Herrera, S. E.; Agazzi, M. L.; Apuzzo, E.; Cortez, M. L.; Marmisollé, W. A.; Tagliazucchi, M.; Azzaroni, O. Polyelectrolyte-Multivalent Molecule Complexes: Physicochemical Properties and Applications. *Soft Matter* **2023**, *19* (11), 2013−2041.

(6) Sing, C. E.; Perry, S. L. Recent Progress in the Science of Complex Coacervation. *Soft Matter* **2020**, *16* (12), 2885−2914.

(7) Wang, Q.; Schlenoff, J. B. The Polyelectrolyte Complex/Coacervate Continuum. *Macromolecules* **2014**, *47* (9), 3108−3116.

(8) Perry, S. L.; Leon, L.; Hoffmann, K. Q.; Kade, M. J.; Priftis, D.; Black, K. A.; Wong, D.; Klein, R. A.; Pierce, C. F.; Margossian, K. O.; Whitmer, J. K.; Qin, J.; de Pablo, J. J.; Tirrell, M. Chirality-Selected Phase Behaviour in Ionic Polypeptide Complexes. *Nat. Commun.* **2015**, *6* (1), No. 6052.

(9) Guo, Q.; Zou, G.; Qian, X.; Chen, S.; Gao, H.; Yu, J. Hydrogen-Bonds Mediate Liquid-Liquid Phase Separation of Mussel Derived Adhesive Peptides. *Nat. Commun.* **2022**, *13* (1), No. 5771.

(10) Hyman, A. A.; Weber, C. A.; Jülicher, F. Liquid-Liquid Phase Separation in Biology. *Annu. Rev. Cell Dev. Biol.* **2014**, *30*, 39−58.

(11) Kim, S.; Huang, J.; Lee, Y.; Dutta, S.; Yoo, H. Y.; Jung, Y. M.; Jho, Y.; Zeng, H.; Hwang, D. S. Complexation and Coacervation of Like-Charged Polyelectrolytes Inspired by Mussels. *Proc. Natl. Acad. Sci. U.S.A.* **2016**, *113* (7), E847−E853.

(12) Brangwynne, C. P.; Tompa, P.; Pappu, R. V. Polymer Physics of Intracellular Phase Transitions. *Nat. Phys.* **2015**, *11* (11), 899−904.

(13) Brangwynne, C. P.; Eckmann, C. R.; Courson, D. S.; Rybarska, A.; Hoege, C.; Gharakhani, J.; Jülicher, F.; Hyman, A. A. Germline P Granules Are Liquid Droplets That Localize by Controlled Dissolution/Condensation. *Science* **2009**, *324* (5935), 1729−1732.

(14) Wang, J.; Choi, J.-M.; Holehouse, A. S.; Lee, H. O.; Zhang, X.; Jahnel, M.; Maharana, S.; Lemaitre, R.; Pozniakovsky, A.; Drechsel, D.; Poser, I.; Pappu, R. V.; Alberti, S.; Hyman, A. A. A Molecular Grammar Governing the Driving Forces for Phase Separation of Prion-like RNA Binding Proteins. *Cell* **2018**, *174* (3), 688−699.

(15) Buddingh, B. C.; van Hest, J. C. M. Artificial Cells: Synthetic Compartments with Life-like Functionality and Adaptivity. *Acc. Chem. Res.* **2017**, *50* (4), 769−777.

(16) Poudyal, R. R.; Guth-Metzler, R. M.; Veenis, A. J.; Frankel, E. A.; Keating, C. D.; Bevilacqua, P. C. Template-Directed RNA Polymerization and Enhanced Ribozyme Catalysis inside Membraneless Compartments Formed by Coacervates. *Nat. Commun.* **2019**, *10* (1), No. 490.

(17) Cao, S.; Ivanov, T.; Heuer, J.; Ferguson, C. T. J.; Landfester, K.; Caire da Silva, L. Dipeptide Coacervates as Artificial Membraneless Organelles for Bioorthogonal Catalysis. *Nat. Commun.* **2024**, *15* (1), No. 39.

(18) van der Gucht, J.; Spruijt, E.; Lemmers, M.; Cohen Stuart, M. A. Polyelectrolyte Complexes: Bulk Phases and Colloidal Systems. *J. Colloid Interface Sci.* **2011**, *361* (2), 407−422.

(19) Spruijt, E.; Westphal, A. H.; Borst, J. W.; Cohen Stuart, M. A.; van der Gucht, J. Binodal Compositions of Polyelectrolyte Complexes. *Macromolecules* **2010**, *43* (15), 6476−6484.

(20) Ortony, J. H.; Choi, S.-H.; Spruell, J. M.; Hunt, J. N.; Lynd, N. A.; Krogstad, D. V.; Urban, V. S.; Hawker, C. J.; Kramer, E. J.; Han, S. Fluidity and Water in Nanoscale Domains Define Coacervate Hydrogels. *Chem. Sci.* **2014**, *5* (1), 58−67.

(21) Lu, T.; Spruijt, E. Multiphase Complex Coacervate Droplets. *J. Am. Chem. Soc.* **2020**, *142* (6), 2905−2914.

(22) Qin, J.; Priftis, D.; Farina, R.; Perry, S. L.; Leon, L.; Whitmer, J.; Hoffmann, K.; Tirrell, M.; de Pablo, J. J. Interfacial Tension of Polyelectrolyte Complex Coacervate Phases. *ACS Macro Lett.* **2014**, *3* (6), 565−568.

(23) Patra, S.; Chandrabhas, S.; Dhiman, S.; George, S. J. Controlled Supramolecular Polymerization via Bioinspired, Liquid−Liquid Phase Separation of Monomers. *J. Am. Chem. Soc.* **2024**, *146* (18), 12577−12586.

(24) Yuan, C.; Levin, A.; Chen, W.; Xing, R.; Zou, Q.; Herling, T. W.; Challa, P. K.; Knowles, T. P. J.; Yan, X. Nucleation and Growth of Amino Acid and Peptide Supramolecular Polymers through Liquid−Liquid Phase Separation. *Angew. Chem., Int. Ed.* **2019**, *58* (50), 18116−18123.

(25) Fu, H.; Huang, J.; van der Tol, J. J. B.; Su, L.; Wang, Y.; Dey, S.; Zijlstra, P.; Fytas, G.; Vantomme, G.; Dankers, P. Y. W.; Meijer, E. W. Supramolecular Polymers Form Tactoids through Liquid−Liquid Phase Separation. *Nature* **2024**, *626* (8001), 1011−1018.

(26) Garenne, D.; Beven, L.; Navailles, L.; Nallet, F.; Dufourc, E. J.; Douliez, J.-P. Sequestration of Proteins by Fatty Acid Coacervates for Their Encapsulation within Vesicles. *Angew. Chem., Int. Ed.* **2016**, *55* (43), 13475−13479.

(27) Tang, T.-Y. D.; Swaay, D.; van de Mello, A.; Anderson, J. L. R.; Mann, S. In Vitro Gene Expression within Membrane-Free Coacervate Protocells. *Chem. Commun.* **2015**, *51* (57), 11429−11432.

(28) Aumiller, W. M., Jr.; Keating, C. D. Phosphorylation-Mediated RNA/Peptide Complex Coacervation as a Model for Intracellular Liquid Organelles. *Nat. Chem.* **2016**, *8*, 129−137.

(29) Yewdall, N. A.; André, A. A. M.; Lu, T.; Spruijt, E. Coacervates as Models of Membraneless Organelles. *Curr. Opin. Colloid Interface Sci.* **2021**, *52*, No. 101416.

(30) Krishna Kumar, R.; Harniman, R. L.; Patil, A. J.; Mann, S. Self-Transformation and Structural Reconfiguration in Coacervate-Based Protocells. *Chem. Sci.* **2016**, *7* (9), 5879−5887.
(31) Madhanagopal, B. R.; Rodriguez, A.; Cordones, M.; Chandrasekaran, A. R. Barium Concentration-Dependent Anomalous Electrophoresis of Synthetic DNA Motifs. *ACS Appl. Bio Mater.* **2024**, *7* (5), 2704−2709.
(32) Lambert, O.; Letellier, L.; Gelbart, W. M.; Rigaud, J.-L. DNA Delivery by Phage as a Strategy for Encapsulating Toroidal Condensates of Arbitrary Size into Liposomes. *Proc. Natl. Acad. Sci. U.S.A.* **2000**, *97* (13), 7248−7253.
(33) Gosule, L. C.; Schellman, J. A. Compact Form of DNA Induced by Spermidine. *Nature* **1976**, *259* (5541), 333−335.
(34) Chattoraj, D. K.; Gosule, L. C.; Schellman, J. A. DNA Condensation with Polyamines: II. Electron Microscopic Studies. *J. Mol. Biol.* **1978**, *121* (3), 327−337.
(35) Angelini, T. E.; Liang, H.; Wriggers, W.; Wong, G. C. L. Like-Charge Attraction between Polyelectrolytes Induced by Counterion Charge Density Waves. *Proc. Natl. Acad. Sci. U.S.A.* **2003**, *100* (15), 8634−8637.
(36) Muthukumar, M. Theory of Counter-Ion Condensation on Flexible Polyelectrolytes: Adsorption Mechanism. *J. Chem. Phys.* **2004**, *120* (19), 9343−9350.
(37) Zheng, Y.; Lin, C.; Zhang, J.-S.; Tan, Z.-J. Ion-Mediated Interactions between like-Charged Polyelectrolytes with Bending Flexibility. *Sci. Rep.* **2020**, *10* (1), No. 21586.
(38) Martin, T. G.; Dietz, H. Magnesium-Free Self-Assembly of Multi-Layer DNA Objects. *Nat. Commun.* **2012**, *3* (1), No. 1103.
(39) Wissenburg, P.; Odijk, T.; Cirkel, P.; Mandel, M. Multimolecular Aggregation in Concentrated Isotropic Solutions of Mononucleosomal DNA in 1 M Sodium Chloride. *Macromolecules* **1994**, *27* (1), 306−308.
(40) Wissenburg, P.; Odijk, T.; Cirkel, P.; Mandel, M. Multimolecular Aggregation of Mononucleosomal DNA in Concentrated Isotropic Solutions. *Macromolecules* **1995**, *28* (7), 2315−2328.
(41) Jain, M.; Seth, J. R.; Hegde, L. R.; Sharma, K. P. Unprecedented Self-Assembly in Dilute Aqueous Solution of Polyethyleneimine: Formation of Fibrillar Network. *Macromolecules* **2020**, *53* (20), 8974−8981.
(42) Sharma, S.; Sharma, K. P. Light-Responsive Self-Assembled Microstructures of Branched Polyethyleneimine at Low pH. *Chem. Commun.* **2022**, *58* (99), 13779−13782.
(43) Muthukumar, M. Ordinary−Extraordinary Transition in Dynamics of Solutions of Charged Macromolecules. *Proc. Natl. Acad. Sci. U.S.A.* **2016**, *113* (45), 12627−12632.
(44) Jia, D.; Muthukumar, M. Dipole-Driven Interlude of Mesomorphism in Polyelectrolyte Solutions. *Proc. Natl. Acad. Sci. U.S.A.* **2022**, *119* (40), No. e2204163119.
(45) Kanai, S.; Muthukumar, M. Phase Separation Kinetics of Polyelectrolyte Solutions. *J. Chem. Phys.* **2007**, *127* (24), No. 244908.
(46) Lopez, C. G.; Horkay, F.; Schweins, R.; Richtering, W. Solution Properties of Polyelectrolytes with Divalent Counterions. *Macromolecules* **2021**, *54* (22), 10583−10593.
(47) Wong, G. C. L.; Lin, A.; Tang, J. X.; Li, Y.; Janmey, P. A.; Safinya, C. R. Lamellar Phase of Stacked Two-Dimensional Rafts of Actin Filaments. *Phys. Rev. Lett.* **2003**, *91* (1), No. 018103.
(48) Drobot, B.; Iglesias-Artola, J. M.; Le Vay, K.; Mayr, V.; Kar, M.; Kreysing, M.; Mutschler, H.; Tang, T.-Y. D. Compartmentalised RNA Catalysis in Membrane-Free Coacervate Protocells. *Nat. Commun.* **2018**, *9* (1), No. 3643.
(49) Horn, J. M.; Kapelner, R. A.; Obermeyer, A. C. Macro- and Microphase Separated Protein-Polyelectrolyte Complexes: Design Parameters and Current Progress. *Polymers* **2019**, *11* (4), 578.
(50) Agrawal, A.; Radakovic, A.; Vonteddu, A.; Rizvi, S.; Huynh, V. N.; Douglas, J. F.; Tirrell, M. V.; Karim, A.; Szostak, J. W. Did the Exposure of Coacervate Droplets to Rain Make Them the First Stable Protocells. *Sci. Adv.* **2024**, *10* (34), No. eadn9657.
(51) Altenburg, W. J.; Yewdall, N. A.; Vervoort, D. F. M.; van Stevendaal, M. H. M. E.; Mason, A. F.; van Hest, J. C. M. Programmed Spatial Organization of Biomacromolecules into Discrete, Coacervate-Based Protocells. *Nat. Commun.* **2020**, *11* (1), No. 6282.
(52) Lippincott-Schwartz, J.; Snapp, E.; Kenworthy, A. Studying Protein Dynamics in Living Cells. *Nat. Rev. Mol. Cell Biol.* **2001**, *2* (6), 444−456.
(53) Perry, S. L.; Li, Y.; Priftis, D.; Leon, L.; Tirrell, M. The Effect of Salt on the Complex Coacervation of Vinyl Polyelectrolytes. *Polymers* **2014**, *6* (6), 1756−1772.
(54) Blocher, W. C.; Perry, S. L. Complex Coacervate-Based Materials for Biomedicine. *WIREs Nanomed. Nanobiotechnol.* **2017**, *9* (4), No. e1442.
(55) Collins, K. D. Ion Hydration: Implications for Cellular Function, Polyelectrolytes, and Protein Crystallization. *Biophys. Chem.* **2006**, *119* (3), 271−281.
(56) Zhang, Y.; Cremer, P. S. Interactions between Macromolecules and Ions: The Hofmeister Series. *Curr. Opin. Chem. Biol.* **2006**, *10* (6), 658−663.
(57) Gajo, C.; Shchepanovska, D.; Jones, J. F.; Karras, G.; Malakar, P.; Greetham, G. M.; Hawkins, O. A.; Jordan, C. J. C.; Curchod, B. F. E.; Oliver, T. A. A. Nile Red Fluorescence: Where's the Twist? *J. Phys. Chem. B* **2024**, *128* (47), 11768−11775.
(58) Herrera, S. E.; Agazzi, M. L.; Cortez, M. L.; Marmisollé, W. A.; Tagliazucchi, M.; Azzaroni, O. Polyamine Colloids Cross-Linked with Phosphate Ions: Towards Understanding the Solution Phase Behavior. *ChemPhysChem* **2019**, *20* (8), 1044−1053.
(59) Vanderzee, C. E.; Quist, A. S. The third dissociation constant of orthophosphoric acid. *J. Phys. Chem. A* **1961**, *65* (1), 118−123.
(60) Ferroni, G. Potentiometric Studies on Association and Dissociation Equilibria of Orthophosphoric Acid, in water KCl 3M Medium at 25°C. *Electrochim. Acta* **1976**, *21* (4), 283−286.
(61) Wang, L.; Nancollas, G. H. Calcium Orthophosphates: Crystallization and Dissolution. *Chem. Rev.* **2008**, *108* (11), 4628−4669.
(62) Yong, H. Reentrant Condensation of Polyelectrolytes Induced by Diluted Multivalent Salts: The Role of Electrostatic Gluonic Effects. *Biomacromolecules* **2024**, *25* (11), 7361−7376.
(63) Singh, R. K.; Gade, H. M.; Sharma, K. P.; Seth, J. R. Entropy-Driven Attraction between Weakly Basic Polyelectrolytes Ionized with Monoprotic Acids. *Macromolecules* **2025**, *58* (6), 3058−3071.
(64) Gallops, C. E.; Yu, C.; Ziebarth, J. D.; Wang, Y. Effect of the Protonation Level and Ionic Strength on the Structure of Linear Polyethyleneimine. *ACS Omega* **2019**, *4* (4), 7255−7264.
(65) Curtis, K. A.; Miller, D.; Millard, P.; Basu, S.; Horkay, F.; Chandran, P. L. Unusual Salt and pH Induced Changes in Polyethylenimine Solutions. *PLoS One* **2016**, *11* (9), No. e0158147.
(66) Koper, G. J. M.; Borkovec, M. Proton Binding by Linear, Branched, and Hyperbranched Polyelectrolytes. *Polymer* **2010**, *51* (24), 5649−5662.
(67) Nagaya, J.; Homma, M.; Tanioka, A.; Minakata, A. Relationship between Protonation and Ion Condensation for Branched Poly(Ethylenimine. *Biophys. Chem.* **1996**, *60* (1), 45−51.
(68) Douyère, G.; Leclercq, L.; Nardello-Rataj, V. From Polyethyleneimine Hydrogels to Pickering-like Smart "On/Off" Emulgels Switched by pH and Temperature. *J. Colloid Interface Sci.* **2022**, *628*, 807−819.
(69) Lin, C.; Qiang, X.; Dong, H.-L.; Huo, J.; Tan, Z.-J. Multivalent Ion-Mediated Attraction between Like-Charged Colloidal Particles: Nonmonotonic Dependence on the Particle Charge. *ACS Omega* **2021**, *6* (14), 9876−9886.
(70) Kenworthy, A. K. What's Past Is Prologue: FRAP Keeps Delivering 50 Years Later. *Biophys. J.* **2023**, *122* (18), 3577−3586.
(71) Aumiller, W. M., Jr.; Cakmak, F. P.; Davis, B. W.; Keating, C. D. RNA-Based Coacervates as a Model for Membraneless Organelles: Formation, Properties, and Interfacial Liposome Assembly. *Langmuir* **2016**, *32* (39), 10042−10053.
(72) Kohze, R.; Dieteren, C. E. J.; Koopman, W. J. H.; Brock, R.; Schmidt, S. Frapbot: An Open-Source Application for FRAP Data. *Cytometry, Part A* **2017**, *91* (8), 810−814.

https://doi.org/10.1021/acs.macromol.5c01505
Macromolecules XXXX, XXX, XXX−XXX